

## Article

# Characterization of Mortar from Casa Barbot (Portugal), a Case Study from the Beginning of the 20th Century

Hamid Maljaee <sup>1,\*</sup>, António Santos Silva <sup>2</sup>  and Ana Velosa <sup>1</sup> 

<sup>1</sup> Civil Engineering Department, RISCO, Campus Universitário de Santiago, University of Aveiro, 3810-193 Aveiro, Portugal

<sup>2</sup> National Laboratory for Civil Engineering, Av. Do Brasil 101, 1700-066 Lisbon, Portugal

\* Correspondence: h.maljaee@ua.pt

**Abstract:** The popularity of natural cement (Roman cement) in buildings from the late 19th and the beginning of the 20th century and the high diversity of characteristics of natural cement demand research of mortar and binders used in the buildings of this period in Portugal. Understanding the type of binder used in the historic buildings will help the project/intervention team to make the best decisions in terms of the development of compatible mortars for historical conservation purposes. Casa Barbot is one of the Art Nouveau examples of the beginning of the 20th century in Portugal. The garden of this building is characterized by peculiar elements in terms of materials and architecture. Full characterization of the mortars employed in the construction of this building as well as identification of the used binder is the main objective of this study. The study comprises a wide range of laboratory characterization techniques such as X-ray fluorescence (XRF), X-ray diffraction (XRD), petrography, open porosity, density, water absorption by capillarity, and compressive strength. The results show the diversity of compositional characteristics in the mortars used in the decorative elements in the period garden of Casa Barbot. All mortars are composed of Portland cement with a mix of additives such as blast furnace slag, limestone filler, air lime, and the occasional presence of charcoal. The results raise doubt about the use of natural cement as stated in the historical documents. This study will broaden the scientific knowledge of the materials of that period in Portugal to provide a comprehensive plan for the preservation of historical buildings.



**Citation:** Maljaee, H.; Silva, A.S.; Velosa, A. Characterization of Mortar from Casa Barbot (Portugal), a Case Study from the Beginning of the 20th Century. *Buildings* **2023**, *13*, 232. <https://doi.org/10.3390/buildings13010232>

Academic Editor: Elena Ferretti

Received: 28 November 2022

Revised: 7 January 2023

Accepted: 11 January 2023

Published: 13 January 2023



**Copyright:** © 2023 by the authors. Licensee MDPI, Basel, Switzerland. This article is an open access article distributed under the terms and conditions of the Creative Commons Attribution (CC BY) license (<https://creativecommons.org/licenses/by/4.0/>).

**Keywords:** 20th century; mortar; Portland cement; Art Nouveau; conservation

## 1. Introduction

The preservation of heritage is an important action that must be performed in order to maintain cultural assets for future generations. This encompasses the intervention on renders and understanding the type of binder used in the historic mortar that helps the material specialist undertake the best decisions in terms of the development of compatible mortars for historical conservation purposes. The architecture of heritage buildings from the late 19th and the beginning of the 20th century ranges from Art Nouveau and Art Deco to Modernism. This period is characterized by the transition of the main construction binder from air lime to Portland cement. In this context, the first cement used is known as natural or Roman cement. Natural cement was patented in 1796 by Reverend James Parker, by calcination of high clay content marlstones (750–1200 °C) without changes in the composition after extraction [1,2]. This type of cement was extensively used all over Europe simulating a cast stone in the execution of decorative elements and as a façade rendering. Depending on the local natural cement production site and firing process, large dispersion can be found in the composition of natural cement which reveals a need for further research.

The nineteenth century witnessed the most important advances in the understanding of hydraulic binders. Air lime, which was in use for many centuries all over the world was

characterized by a very slow hardening and strength-gaining process despite its great long-term performance as could be seen in Joanina Tower of Sra. da Luz fortress in Portugal [3] and military forts in maritime environments [4], among a vastitude of others. Air lime mortars were used in construction from immemorial times until at least the first decades of the 20th century [5,6]. Since Roman times, there was an attempt to improve the water resistance and durability of lime mortars by adding pozzolans [7]. However, a need for quicker hardening and higher strength caused the discarding of air lime-based mortars in the following centuries. Hydraulic lime was first produced by calcining blue Lias limestone containing clay by James Smeaton. These hydraulic binders were obtained by mixing lime with pozzolans, enabling hardening by the addition of water [8]. Lime-based mortars were then overthrown in terms of use by the new hydraulic binders—natural or Roman cement. The term “natural” in natural cement comes from the fact that all the necessary oxides such as lime, silica, alumina, etc., can be found in a unique source material rather than in a material mix from different sources, as is the case of Portland cement. Natural cement received preference over the other hydraulic binders in that period for several reasons. The use of natural cement was quickly spread all over Europe and many quarries were discovered following the demand for fire-resistance and durable stucco-like finishes in the façade resembling the natural stones in the 17th and 18th centuries. Moreover, the quick setting was one of the major reasons why natural cement could fit adequately into the 20th-century demands, particularly for repair and running moldings [9].

The use of natural cement in Portugal dates back to the second half of the 19th century and the beginning of the 20th century [10]. The effective industrial production of natural cement began in 1866 in *Alcântara*, Lisbon [11]. However, there is a lack of well-documented evidence about the production and use of natural cement in Portugal. During this period, this cement was massively used in Europe to produce cast stone and decorative ornaments to simulate natural stone due to their brownish color [12,13]. This period also coincides with the invention and development of Portland cement. Portland cement was created by Joseph Aspdin in 1824 and its name was taken from the Isle of Portland in Dorset, United Kingdom. Following the rising interest in Portland cement and the improvement of technology, the Portuguese industries started the production of Portland cement in 1894 [14], and the use of natural cement and hydraulic lime has been replaced gradually by Portland cement.

Understanding the type of binder is a key step in the restoration of historic buildings. Consecutive previous attempts of renovations with improper high abrasion cleaning methods and inappropriate use of Portland cement led to the loss of details on the façades and aesthetical disfiguring. All these reasons lead to the complication of evaluation of the used binder and eventually the current course of conservation [15]. Differences between natural cement and Portland cement must be taken into account before any restoration action. Indeed, the final properties of natural cement depend on the geological location of marlstones yielding distinct characteristics in terms of color and chemical composition. Natural hydraulic lime and natural cement are often required in restoration practice rather than Portland cement, due to their favorable composition and physical properties that make them more compatible with traditional construction materials such as natural stone. The production of natural cement at lower temperatures avoids the formation of tricalcium silicate (alite), which is responsible for the early age strength development in Portland cement, and due to the high clay content, the main hydraulic phase is belite [15–17]. Furthermore, the presence of calcium aluminate phases is also associated with early strength development and rapid hardening in natural cement or with the hydration and hardening of dehydroxylated clay minerals in the presence of hydrated lime [18]. For this reason, natural cement was often used in exterior decorative elements such as ornaments that require rapid setting and high weathering resistance.

In comparison to the lime-based ancient mortars [3,5–7,19–21], few studies have been devoted to the characterization of binder in the period of the 19th and 20th centuries [16,22–27]. In Portugal, this is also the case as the first building to be evaluated in terms of 20th Century

mortars' characterization was Teatro Nacional de São João [28] and, for intervention purposes, the development of compatible mortars [29] was a stepping stone towards the present study. In the case of Teatro Nacional de São João natural cement, mortars were employed in a cement–lime mix.

The paper aims at the characterization of mortars used in the construction of Casa Barbot, a stylish building from the beginning of the 20th century in Portugal that may represent according to art history the application of natural cement in the cast decorative elements. Different techniques were used to characterize the historic mortars with the main focus on their binder. Phase analytical tools, such as X-ray diffraction (XRD), provide preliminary information on the type of binder used in the historic mortars. The mineral components, textures, and microstructure of hydrated and anhydrous binder, the porosity and type of aggregates used in the mortar, and their proportion in the mortar composition are studied using petrography. The physical, mechanical, and water transfer properties are also assessed in this paper in order to provide physical and mechanical characteristics, mandatory for the compatibility assessment of replacing materials.

## 2. Description of Case Study

Casa Barbot, representing the only specimen of Art Nouveau in the Municipality of Vila Nova de Gaia, near Oporto (Portugal), was built by Bernardo Pinto Abrunhosa in 1904 and is located in the Avenida da Republica which is nowadays considered as the main artery of the city. The name “Casa Barbot” was given when the house was bought by Ermelinda Vilano Barbot and her family in 1944. The building has all the elements such as wrought iron, glass, and tile combined with stonework and thematic levels that characterize Art Nouveau in terms of materials. The Art Nouveau building is also completed by a typical garden, with greenhouses, a small lake, and caves. Casa Barbot and its gardens constitute a unit impacting the historical, architectural, and artistic profile that needs to be preserved with utmost importance. A general intervention in the garden was performed in 1988. Figure 1 shows the main façade of the building, the garden, and its cave-like structure Casa Barbot.



**Figure 1.** The main façade, garden, and caves of the Casa Barbot in Vila Nova de Gaia.

## 3. Sampling and Methods

Mortar samples were collected from the decorative elements of Casa Barbot for compositional characterization. The samples included the detached pieces and those taken from

the cracked regions on the cave structure and gazebo in the period garden of this house by means of chisel and hammer, see the location of collected samples in Figure 2.



**Figure 2.** Samples identification and location in the garden and caves of the Casa Barbot in Vila Nova de Gaia.

The visual inspection revealed the existence of several layers, including inner (denoted as Int), outer (denoted as Ex), and interface layer (denoted as Ins). The description of the taken samples and their stratigraphy are presented in Table 1. Biological colonization could be observed in some samples. Efflorescence was observed on the surface of CB1 (taken from the ceiling of the caves). The samples with embedded rebars show weathering degradation and cracks due to the corrosion of reinforcement. All defects observed are related to the water infiltration through the cave's ceiling or corrosion of the reinforcement.

Tests adopted in this study include XRD, X-ray fluorescence (XRF), petrographic analysis, compressive strength, open porosity, and capillary water absorption. Depending on the type of test adopted, the samples were carefully extracted from each layer.

The samples collected from Casa Barbot were received wet because they have been exposed to the rain and humid weather, thus they first dried in an oven at 100 °C for 24 h. They were then disaggregated and ground (<106 µm) and after prepared as fused beads. The sample analysis was determined by XRF on a Philips X0Pert PRO MPD spectrometer (Amsterdam, Netherlands).

The mineralogical composition of the samples was studied using X-ray diffraction (XRD). The data were collected using X'Pert Pro MPD Panalytical diffractometer equipped with Cu-K $\alpha$  radiation ( $\lambda = 1.5405 \text{ \AA}$ ) operating at 40 mA and 45 kV. The  $2\theta$  scanning was conducted between 3° and 70° at a scan speed of 0.02 /s. Two types of fractions were prepared for XRD: an overall fraction corresponding to the samples as collected and obtained by grinding to pass through a 106 µm sieve, and a fine fraction, which has a higher binder concentration and was obtained by extracting the fines passing a 106 µm sieve directly from the bulk mortar. Fine fraction was only used for XRD analysis. The qualitative mineralogical analysis was completed using the HighScore Plus software from Malvern Panalytical. Semiquantitative XRD analysis was completed by Rietveld phase analyses on the overall fraction and using the structural data from the Crystallography

Open Database (COD) [30–36]. The mineralogical phases identified in this study and the corresponding COD codes are presented in Table 2.

**Table 1.** The sample description.

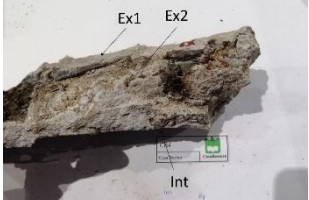
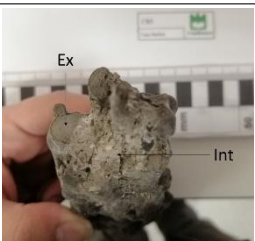
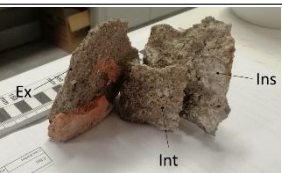
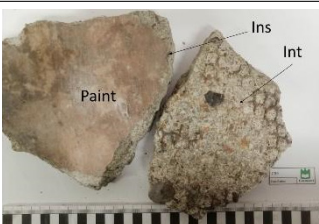
ID	Description	Defects	Stratigraphy
CB1	Coating of the ceiling of the cave in the garden	Efflorescence on the surface	
CB2	Phytomorphic element in the cave	Rebar corrosion	
CB3	Phytomorphic element in the cave	Rebar corrosion	
CB4	Part of beam shape connection in top of the cave	Rebar corrosion	
CB5	Phytomorphic element in the cave (chandelier)	—	
CB6	Part of the connection on top of the cave	—	
CB9	A piece of cave ceiling with meshing	Rebar corrosion	

Table 1. Cont.

ID	Description	Defects	Stratigraphy
CB10	A piece of unknown origin	Rebar corrosion	
CB11	Balustrade of gazebo	–	

Table 2. Mineralogical phases identified and COD identification.

Phases	Formulae	COD Code
Quartz	SiO <sub>2</sub>	9012601
Microcline	KAlSi <sub>3</sub> O <sub>8</sub>	9004192
Albite	NaAlSi <sub>3</sub> O <sub>8</sub>	1556999
Orthoclase	KAlSi <sub>3</sub> O <sub>8</sub>	9006347
Muscovite	KAl <sub>2</sub> (Si <sub>3</sub> Al)O <sub>10</sub> (OH,F) <sub>2</sub>	9004412
Biotite	K(Mg,Fe <sup>2+</sup> ) <sub>3</sub> AlSi <sub>3</sub> O <sub>10</sub> (OH,F) <sub>2</sub>	9000026
Kaolinite	Al <sub>2</sub> Si <sub>2</sub> O <sub>5</sub> (OH) <sub>4</sub>	9009231
Clinocllore	(Mg,Fe <sup>2+</sup> ) <sub>5</sub> Al(Si <sub>3</sub> Al)O <sub>10</sub> (OH) <sub>8</sub>	9013853
Hematite	Fe <sub>2</sub> O <sub>3</sub>	9000140
Calcite	CaCO <sub>3</sub>	9000966
Portlandite	Ca(OH) <sub>2</sub>	1001769
Gypsum	CaSO <sub>4</sub> ·2H <sub>2</sub> O	5000040
Gehlenite	Ca <sub>2</sub> Al <sub>2</sub> SiO <sub>7</sub>	9004072
Alite (C3S)	Ca <sub>3</sub> SiO <sub>4</sub> O	1540705
Belite (C2S)	Ca <sub>3</sub> SiO <sub>4</sub>	9012795
Aluminate (C3A)	Ca <sub>3</sub> Al <sub>2</sub> O <sub>6</sub>	1000040
Ferrite (C4AF)	Ca <sub>2</sub> (Al,Fe <sup>3+</sup> ) <sub>2</sub> O <sub>5</sub>	9003354
Ettringite	Ca <sub>6</sub> Al <sub>2</sub> (SO <sub>4</sub> ) <sub>3</sub> (OH) <sub>12</sub> ·26H <sub>2</sub> O	9015085
Hydrocalumite	Ca <sub>2</sub> Al(OH) <sub>7</sub> ·6.5H <sub>2</sub> O	9009354

Petrographic analysis was adopted as the most efficient tool for analysis of the microstructure of the binder and aggregates in the sampled materials and for identifying its composition. Thin and polished sections of the samples were prepared with vacuum impregnation with a yellow epoxy resin. These were observed on an Olympus BX60 polarizing microscope using transmitted light.

Due to the non-standard and irregular dimension of the collected samples, specific test methods that are developed and validated in previous scientific works [37–39] have been adopted in this study to characterize mechanical and physical properties of mortars. Compressive strength following EN1015-11 [40] was carried out on the samples that were carefully cut in specific dimensions between 20 and 40 mm based on the size of the extracted sample from the case studies. They were then tested using SHIMADZU AG-IC 100 kN at the rate of 500 N/s.

The water absorption by capillarity was performed according to the test procedure described in the EN 15801 [41] which was adapted for irregular and friable samples [37]. The total open porosity and real density were evaluated through immersion and hydrostatic weighing, based on EN 1936 [42].

## 4. Experimental Results and Discussion

### 4.1. Chemical Composition

The chemical composition of samples collected from the caves and garden of Casa Barbot are presented in Table 3.

**Table 3.** Chemical composition of samples from Casa Barbot (wt%).

	CaO	SiO <sub>2</sub>	Al <sub>2</sub> O <sub>3</sub>	Fe <sub>2</sub> O <sub>3</sub>	MgO	SO <sub>3</sub>	K <sub>2</sub> O	P <sub>2</sub> O <sub>5</sub>	Cl	TiO <sub>2</sub>	Na <sub>2</sub> O
CB1-Ex	55.57	28.66	2.33	6.83	0.32	0.79	3.38	0.85	nd	0.74	0.04
CB1-2-Ex	63.07	22.14	2.18	6.27	0.23	0.96	3.08	0.70	0.05	0.64	nd
CB2-Ex	74.89	9.77	1.00	4.51	0.28	4.55	3.41	0.46	0.32	0.44	nd
CB3-Ex1	75.10	12.61	1.23	5.60	0.21	1.81	1.34	0.80	0.09	0.68	0.06
CB3-Ex2	75.76	13.05	1.29	5.46	0.26	0.76	1.68	0.51	0.03	0.58	nd
CB4-Ex	66.32	18.44	1.45	8.83	0.20	1.45	1.83	0.54	0.12	0.44	0.03
CB5-Ex	76.99	7.85	1.53	8.25	0.45	2.27	0.72	0.45	0.30	0.76	nd
CB6-Ex	54.81	26.44	2.55	7.12	0.15	3.20	3.74	0.66	nd	0.72	nd
CB10-Ex	67.13	18.03	1.47	8.10	0.18	0.18	1.45	0.53	0.09	0.66	nd
CB11-Ex	57.58	28.60	1.98	6.30	0.17	0.99	2.35	0.79	0.08	0.76	nd
CB1-Ins	63.33	22.42	2.33	6.50	0.34	0.42	2.91	0.67	nd	0.61	nd
CB6-Ins	56.07	27.16	2.46	7.78	0.13	1.35	2.76	0.74	0.23	0.80	nd
CB9-Ins	71.37	17.02	1.64	5.00	0.16	0.65	2.44	0.54	0.12	0.55	nd
CB1-Int	8.73	58.76	8.09	8.90	0.17	0.14	12.30	1.67	nd	0.62	0.04
CB2-Int	56.64	23.18	1.66	8.63	0.21	1.59	5.43	0.63	0.44	0.56	nd
CB3-Int	65.04	21.25	1.84	5.95	0.22	0.58	3.16	0.71	nd	0.63	nd
CB4-Int	62.05	22.53	1.73	7.72	0.19	0.57	3.01	0.60	0.03	0.51	0.03
CB5-Int	68.80	16.48	1.89	6.21	0.14	1.53	2.76	0.55	0.19	0.59	0.03
CB5-Int	67.63	16.92	1.85	6.46	0.16	1.69	2.72	0.99	0.18	0.57	nd
CB6-Int	40.27	36.64	5.35	7.35	0.12	0.59	6.94	1.45	0.03	0.73	nd
CB9-Int	73.58	14.81	1.45	4.54	0.17	0.66	2.48	0.71	0.45	0.53	0.04
CB10-Int	68.08	16.12	1.98	8.63	0.13	0.94	1.46	0.50	0.19	0.71	0.03
CB11-Int	54.64	29.48	2.36	7.35	0.51	1.24	2.30	0.64	0.24	0.75	nd

The studied mortars dominantly consist of calcium oxide (except for CB1-Int) ranging from 40.27% in CB6-Int to 76.99% in CB5-Ex. A high level of CaO may imply the presence of lime in the binder of these mortars. This will be discussed later in XRD and petrographic analysis. CB1-Int shows the lowest content of calcium oxide and the highest percentage of silica, alumina, and potassium oxide. A reason for such observation could be due to the use of high content of K-feldspar. Complementary techniques such as XRD and optical microscopy could help better understand the compositional characterization of CB1-Int.

The second main oxide composition in the CB mortars is silica. Interestingly, the lowest silica content was observed in the outer layer of CB2 and CB5, both taken from the same region inside the cave, which raises the hypothesis of the use of the same mortar in the elements of this region.

In general, the mortars employed in the exterior layers show higher sulfates (expressed as SO<sub>3</sub>) than those used in the interface and interior layers. This is well related to the direct exposure of the outermost layer to atmospheric pollution which promotes the sulfate attack [43–47]. The highest content of sulfates (4.55%) was observed in CB2-Ex.

Mortar samples present alumina contents ranging from 1.00% in CB2-Ext to 8.09% in CB1-Int, and potassium oxide contents ranging from 0.72% in CB5-Ex to 12.30% in CB1-Int. The presence of feldspars in the composition of the mortar may explain these observations.

All the samples show high content of ferric oxide (Fe<sub>2</sub>O<sub>3</sub>). One of the reasons can be due to the corrosion of embedded rebars as was observed in Table 1. A more complete explanation is given in Section 4.3.

Some samples present chlorine which can be attributed to the external environment. The building is located about 6 km from the Atlantic Ocean and is therefore in a chloride-rich environment.

#### 4.2. Mineralogy

Figures 3–5 illustrate the XRD diffractograms of the external, internal, and intersectional layers of mortars (overall fraction), respectively. The main minerals identified are quartz, calcite, and feldspars (k- and Na-). In mortars CB2-Ex and CB5-Ex the quartz peak is lower than in the other samples, which is indicative of a lower content of siliceous sand. On the other hand, portlandite was only observed in CB4-Ex and CB11-Int mortars. It can be due to either the presence of air lime or Portland cement in the binder. Samples CB10 and CB11 contain ettringite, which coincides with the absence of gypsum, probably due to the full consumption of gypsum with free alumina.

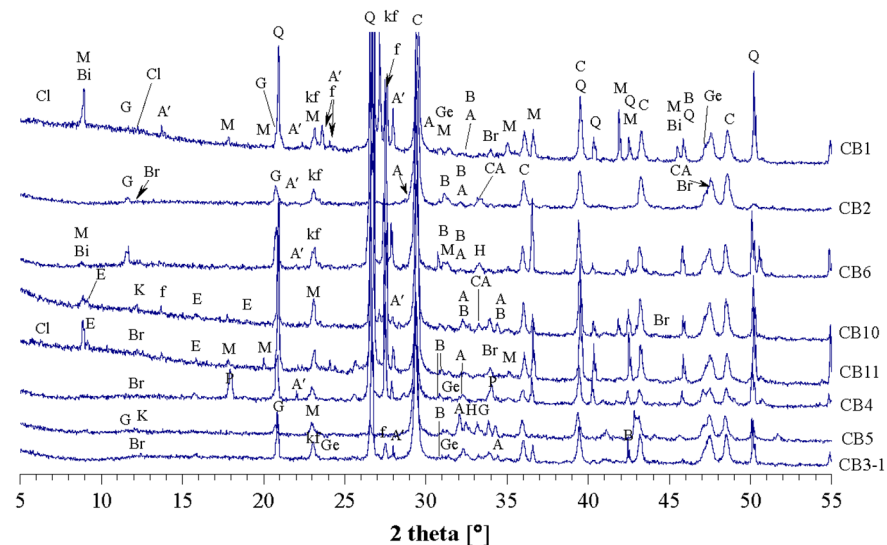


**Figure 3.** XRD diffractograms of the external layer of CB samples (visible peaks that are not labeled with any abbreviation are considered to have the same crystalline compound as the other samples in the same location). Q = quartz, f = feldspar, kf = microcline, A' = albite, E = ettringite, M = muscovite, Bi = biotite, G = gypsum, Br = brownmillerite (C4AF), K = kaolinite, P = portlandite, Ge = gehlenite, B = belite (C2S), A = alite (C3A), H = hematite, Cl = clinochlore, Hc = hydrocalumite, CA = C3A, C = calcite.

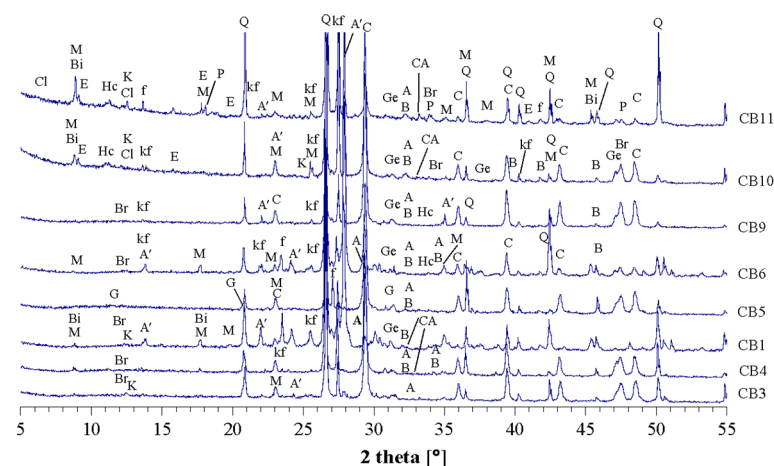


**Figure 4.** XRD diffractograms of the internal layer of CB samples (for the notation see the description in Figure 3).

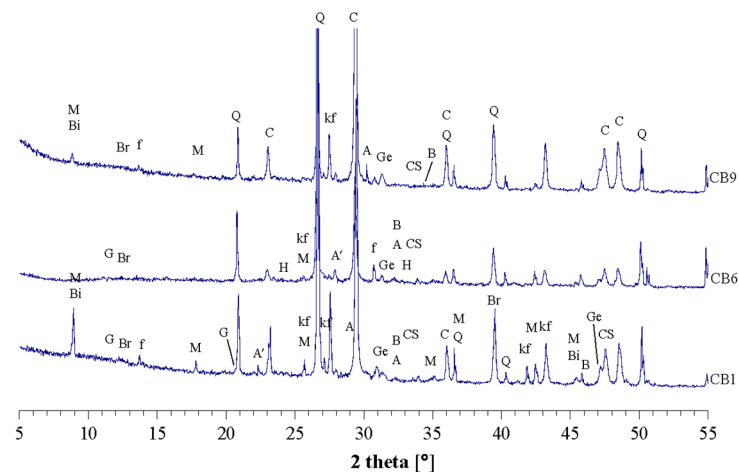


**Figure 5.** XRD diffractograms of intersectional layer of CB samples (for the notation see the description in Figure 3).

It was only possible to prepare a limited quantity of samples for the analysis of the binder-rich fraction. From the analysis of Figure 6, it is evident that the occurrence of Portland clinker phases ( $C_2S$ ,  $C_3S$ ,  $C_4AF$ ) indicates the use of Portland cement in the binder of CB mortars. In some samples, gehlenite ( $Ca_2Al_2SiO_7$ ), a mineral phase that can be attributed to a natural cement [29] or to the use of slags [48], was also detected.

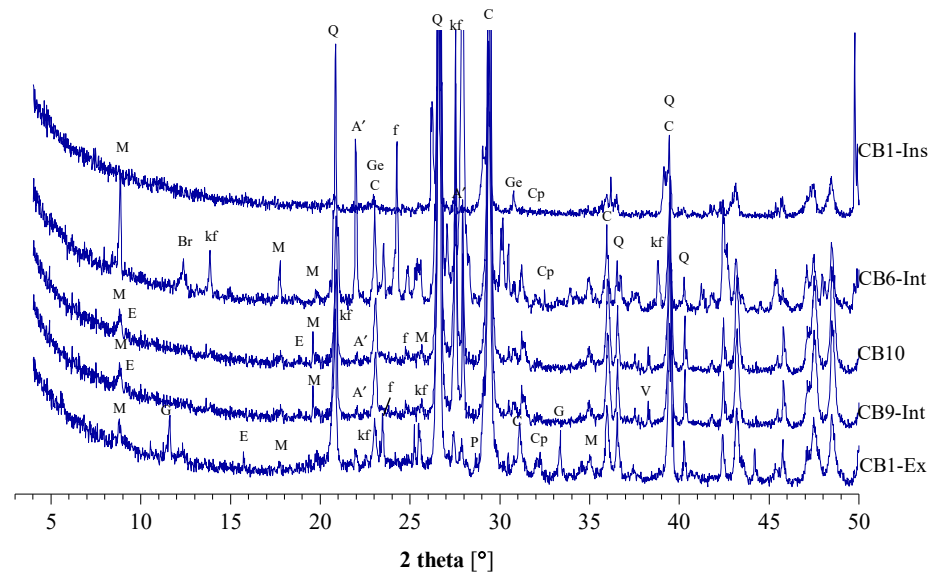


**Figure 6.** XRD diffractograms of binder-rich fraction of CB samples Cp = Portland clinker minerals  $C_3S$  and  $C_2S$  (for the complete notation see the description in Figure 3).

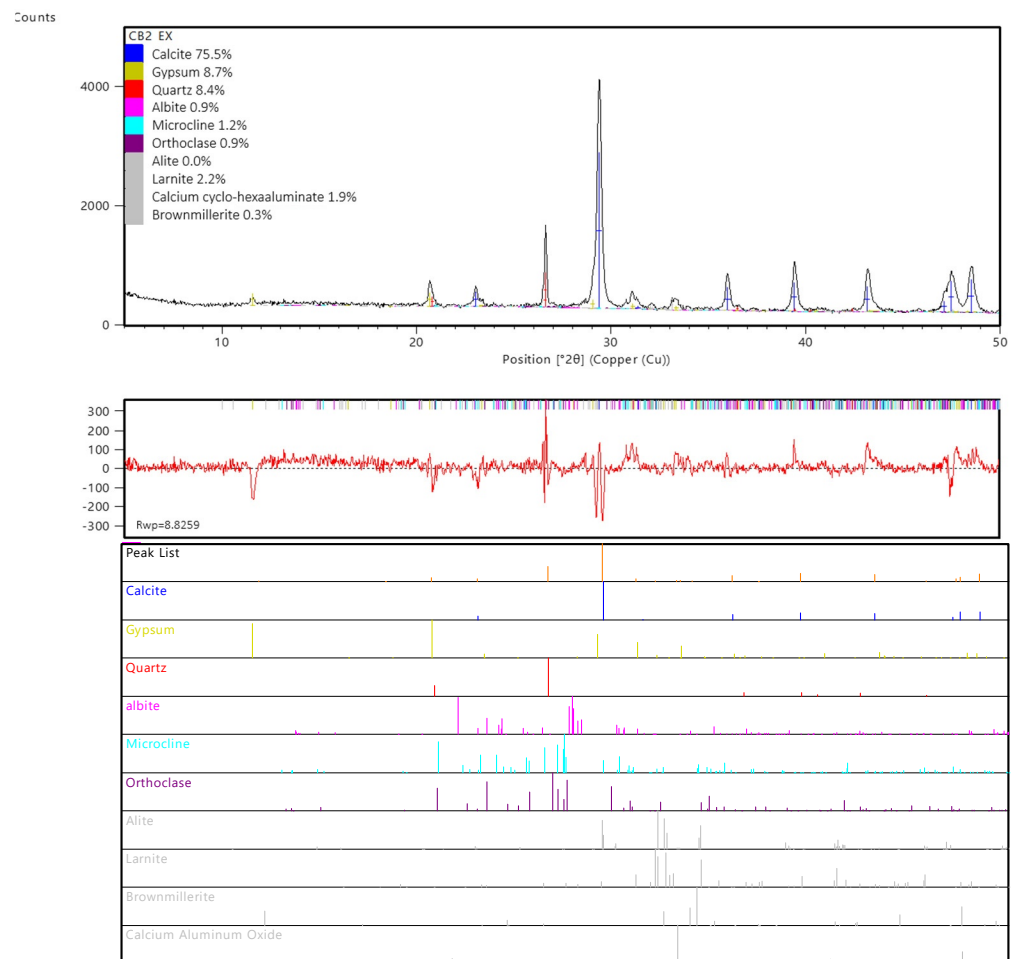
Gypsum is mainly present in the exterior and intersectional layers of mortars which can be attributed to their sulfation [43].

Table 4 shows the semiquantitative results obtained by Rietveld analysis and in Figure 7 an example of XRD pattern fitting and the value of weight profile R-factor (Rwp) is presented.

**Table 4.** XRD composition of CB samples by Rietveld method (overall fractions; wt%).

	CB1-2-Ex	CB1-Ex	CB2-Ex	CB3-Ex1	CB3-Ex2	CB4-Ex	CB5-Ex	CB6-Ex	CB10-Ex	CB11-Ex	CB1-Ins	CB5-Ins	CB9-Ins	CB1-Int	CB3-Int	CB4-Int	CB5-Int	CB6-Int	CB9-Int	CB10-Int	CB11-Int
Quartz (SiO <sub>2</sub> )	30.2	43.9	8.4	26.0	12.6	34.2	2.5	43.8	29.8	55.1	32.6	55.2	26.0	37.5	31.9	35.5	26.3	25.5	14.8	29.3	56.1
Feldspar—microcline (KAlSi <sub>3</sub> O <sub>8</sub> )	11.8	11.9	1.2	4.6	1.9	10.8	0	12.0	16.9	9.2	12.7	3.4	8.6	11.6	10.7	12.0	9.2	6.6	9.8	16.4	16.6
Feldspar—albite (NaAlSi <sub>3</sub> O <sub>8</sub> )	3.7	3.9	0.9	2.7	1.2	11.7	0.6	6.3	1.5	2.4	1.3	4.2	2.0	38.4	3.7	1.5	1.8	41.7	5.6	8.7	6.9
Feldspar—orthoclase (KAlSi <sub>3</sub> O <sub>8</sub> )	0.9	2.9	0.9	0	0.4	3.8	0.2	0	0	0	0	2.1	0	5.7	0	1.4	1.7	6.2	2.1	0	0
Mica—muscovite (KAl <sub>2</sub> (Si <sub>3</sub> Al)O <sub>10</sub> (OH,F) <sub>2</sub> )	1.5	2.0	0	0	1.0	0	0.5	2.0	0	2.4	2.4	0	0.8	5.5	1.1	1.3	0	4.1	0	1.9	3.1
Mica—biotite K(Mg,Fe <sup>2+</sup> ) <sub>3</sub> AlSi <sub>3</sub> O <sub>10</sub> (OH,F) <sub>2</sub>	2.6	3.1	0	0	1.1	0	0.7	1.0	2.2	2.3	3.0	0	1.3	0	0.7	1.1	0	0	0	1.6	3.5
Kaolinite (Al <sub>2</sub> Si <sub>2</sub> O <sub>5</sub> (OH) <sub>4</sub> )	0	0	0	0	1.4	0	1.1	0	0*	0	0	0	0	0*	0.5	0	0	0	0	0	0*
Clinocllore (Mg,Fe <sup>2+</sup> ) <sub>5</sub> Al(Si <sub>3</sub> Al)O <sub>10</sub> (OH) <sub>8</sub>	0.5	0	0	0	0	0	0	0	0	0	0	0	0	0	0	0	0	0	0	0	0*
Hematite (Fe <sub>2</sub> O <sub>3</sub> )	0	0	0	0.1	0	0	0.1	0	0	0	0	0.1	0	0	0	0	0	0	0	0	0
Calcite (CaCO <sub>3</sub> )	47.5	31.2	75.5	56.3	76.2	34.0	61.2	34.0	43.8	26.5	45.9	29.9	58.4	1.2	49.7	45.7	57.4	15.8	64.2	39.1	8.5
Portlandite (Ca(OH) <sub>2</sub> )	0	0	0	0	0	0	0	0	0	0	0	0	0	0	0	0	0	0	0	0	0.7
Gypsum (CaSO <sub>4</sub> ·2H <sub>2</sub> O)	1.2	0.4	8.7	0	0	0	7.2	0	0	0	1.1	0	0	0	0	0	1.9	0	0	0	0
Gehlenite (Ca <sub>2</sub> Al <sub>2</sub> SiO <sub>7</sub> )	0	0.6	0	1.5	1.9	1.0	0	0	0	0	1.1	2.6	2.6	0	1.4	1.1	0	0*	2.6	0*	0*
C3S (Ca <sub>3</sub> SiO <sub>4</sub> )	0*	0*	0*	2.4	0*	0.4	8.5	0*	2.1	0.2	0*	0.3	0.1	0*	0*	0.2	0.2	0	0	0.2	0.2
C2S (Ca <sub>2</sub> SiO <sub>4</sub> )	0*	0*	2.2	3.2	0.3	1.3	12.9	0*	0.4	0*	0*	1.6	0	0*	0*	0	0.9	0*	0.5	0*	
C3A (Ca <sub>3</sub> Al <sub>2</sub> O <sub>6</sub> )	0*	0.1	1.9	1.3	1.5	0	3.2	0.9	1	0.3	0*	0.2	0.2	0	0.4	0.1	0.6	0*	0.4	0.2	
C4AF (Ca <sub>2</sub> (Al,Fe <sup>3+</sup> ) <sub>2</sub> O <sub>5</sub> )	0*	0*	0.3	1.9	0.5	2.9	1.4	0*	0	0.1	0*	0.4	0	0*	0	0	0	0*	0*	0*	0*
Etringite (Ca <sub>6</sub> Al <sub>2</sub> (SO <sub>4</sub> ) <sub>3</sub> (OH) <sub>12</sub> ·26(H <sub>2</sub> O)	0	0	0	0	0	0	0	0	2.2	1.4	0	0	0	0*	0	0	0	0*	0*	2.2	3.1
Hydrocalumite (Ca <sub>2</sub> Al(OH) <sub>7</sub> ·6.5H <sub>2</sub> O)	0	0	0	0	0	0	0	0	0	0	0	0	0	0*	0	0	0	0	0*	0.4	0.6

\* Indicates that the mineral exists in very low content and its quantification is doubtful.

**Figure 7.** XRD diffractogram of sample CB2-Ex showing the fit result obtained by Rietveld refinement.

The XRD analysis shows that the predominant component is calcite. The calcite content in the external and intersectional layers ranged from 26.5 to 76.2%. However, lower calcite was found in the internal layers (from 1.2% in CB1-Int to 64.2% in CB9-Int). The main minerals of the aggregates are quartz, feldspars (namely microcline, albite,

and orthoclase), mica (muscovite and biotite), and the occasional presence of kaolinite, clinocllore, and hematite. According to the XRD results, the aggregates seem to be of an igneous/metamorphic origin, which are the predominant types in the outcrops in the area. Since the aggregates are siliceous, the high content of calcite can be attributed to the presence of lime and to high binder carbonation (see Section 4.3). For the same reason, the lower content of calcite in the internal layers is consonant with the lower CO<sub>2</sub> penetration.

#### 4.3. Petrography

The petrographic analysis was carried out on samples CB1, CB5, and CB11, considered representative of the mortars used in the construction of Casa Barbot. A summary of the main petrographic characteristics of the samples is presented in Table 5.

**Table 5.** Summary of the petrographic analysis (AL = air lime, PC = Portland cement, HL = hydraulic lime, BFS = blast furnace slag).

		Color	Quartz	Feldspar	Quartzite	Limestone	Others	Grain Shape	Particle Size	AggreGate Ratio (Vol%)	Binder Type	Lime Lumps	Binder Ratio (Vol%)	Air Void (Vol%)	Observations
CB1	Outermost paint layer	Black	✓	—	—	✓	—	—	<30 μm	—	AL, PC	—	—	—	Remnants of the layer
	CB1-Ext: Mortar 2 splash plaster	Greyish brown	✓	✓	✓	✓	✓	Sub-angular	≤1.8 mm	47	PC, HL, AL	✓	50	3	Very uneven surface, fully carbonated
	CB1-Int: Mortar 1	Greyish brown	✓	✓	✓	✓	✓	Sub-angular	≤5.2 mm	52	PC, HL, AL	✓	47	1	Partially carbonated, Contains BFS
CB5	Outermost paint layer 2	Orange	—	—	—	—	—	—	—	—	AL	—	—	—	Remnants
	Paint layer 1	Black	✓	—	—	✓	—	—	<25 μm	—	AL, PC	—	—	—	—
CB11	CB5-Ext: Mortar 3	Greyish brown	—	—	—	—	—	—	—	—	PC, AL, HL	✓	99	1	Fully carbonated
	CB5-Ins: Mortar 2	Light grey	✓	✓	✓	✓	✓	Sub-angular	≤2 mm	32	PC, HL, AL	✓	38	4	Fully carbonated
	CB5-Int: Mortar 1	Light grey	✓	✓	✓	✓	✓	Sub-angular	≤1.6 mm	55	PC, HL, AL	✓	43	2	Fully carbonated
	Mortar 3 splashes	Grey	✓	✓	✓	✓	✓	Sub-angular	≤0.6 mm	—	PC	—	—	—	Fully carbonated
	CB11-Ext: Mortar 2	Reddish	—	—	—	—	—	—	—	—	PC, AL, HL	✓	—	—	Fully carbonated
CB11-Int: Mortar 1	Grey	✓	✓	✓	✓	✓	Sub-angular	≤3.2 mm	49	PC, AL, HL	✓	50	1	Partially carbonated, Contains BFS	

This analysis showed a variety of aggregates, confirming the XRD results (see Section 4.2). All studied samples show aggregates mainly consisted of quartz and quartzite with a minor amount of metasiltstone including mica (muscovite) and feldspar, as was confirmed by both XRD and XRF techniques (where a high percentage of potassium was detected). Rounded to sub-angular grains of bituminous sedimentary limestone (Figure 8) were observed in the composition of all samples as a filler, except for the exterior layer of CB5 (labeled as “Mortar 3” in Figure 8). Small black charcoal-like particles with fragments of up to 0.08 and 0.1 mm in size were observed in the composition of all mortars (Figure 8), accounting for less than 1 vol% of the binder.

As Table 5 shows, the binder of all the analyzed mortars is partial to fully carbonated. This observation in conjunction with the presence of limestone filler grains explains the high contents of CaO in XRF and calcite in XRD analysis.

A mix of different materials including Portland cement, hydraulic lime, air lime, blast furnace slag, and limestone filler are observed in the binder paste of the internal layer of CB1 (CB1-Int), see Figure 8b. While the external layer of CB1 was fully carbonated, the internal layer showed only carbonated binder to a depth of less than 1 mm and up to 4 mm. The presence of blast furnace slag, which is rich in silica and alumina was further proven by XRF results, in which the content of silica and alumina was the highest among all mortars.

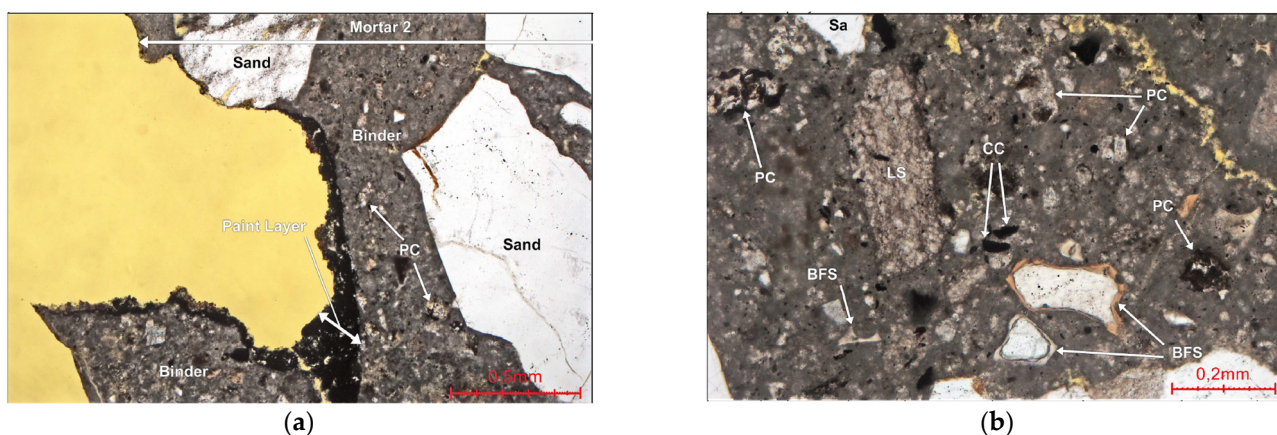


**Figure 8.** Micrographs in polarized light of CB1 sample: (a) external layer which shows remnants of a black paint layer on the surface of the outermost layer of splash render (Mortar 2). The binder of the paint layer consists of a mix of Portland cement and air lime. The mortar contains charcoal (CC-black particles), and the binder presents a high content of Portland clinker grains (PC); (b) interior layer whose binder paste consists of a mixture of Portland cement (PC), grains of limestone (LS), blast furnace slags (BFS) and lime (not seen on the photo). Small fragments of charcoal (CC) give the mortar a rather dark color. Sand aggregates = Sa. The thin section was impregnated with yellow epoxy resin.

The binder of an uneven splash render mortar of CB1 (which can be seen all over the ceiling of the cave) appears to be a mix of Portland cement and lime. Several types of air and hydraulic lime lumps are present, namely rounded to sub-angular lumps of microcrystalline lime without any impurities, light brownish to brownish rounded lumps of microcrystalline lime with low content of impurities, and brownish to greyish lumps and grains of lime with high content of impurities.

A black paint layer of carboniferous pigment is also present over the surface of the splash render. The binder is a mix of air lime and Portland cement and is partly transformed into gypsum.

A reason for the relatively high content of ferric oxide obtained by XRF analysis could be explained by the presence of rounded lumps and grains of microcrystalline lime with high content of impurities in the form of brownish iron-rich clay compounds. Grayish, sub-rounded grains of partly hydrated  $C_4AF$  were also seen in the composition of the binder of CB1 mortar samples.

Sample CB5 (Figure 9) has two paint layers, an orange air lime paint on the exterior over a black carboniferous layer made with a mix of air lime and Portland cement. The interior mortar layer (CB5-Int) is a mix of Portland cement–air lime–hydraulic lime, with limestone filler and black charcoal particles. The hydraulic lime was attributed to the presence of lumps and grains of lime with high content of impurities in form of amorphous to microcrystalline silicate phases. The intermediate (CB5-Ins) and external (CB5-Ext) layers present the same type of binder, which is composed of a mix of air and hydraulic lime with Portland cement. These mortar layers are fully carbonated.

Sample CB11 is stratigraphically very similar to CB5, although it has no layers of paint (Figure 10). In terms of binder, the splashed layer (CB11-Ext) is a Portland cement mortar. The second layer is a reddish render made by a mix of air and hydraulic lime with Portland cement. The color of this render is due to a red iron oxide pigment. The innermost layer (CB11-Int) is grayish, and the binder is also a mix of Portland cement with lime (air and hydraulic), together with some blast furnace slag grains.

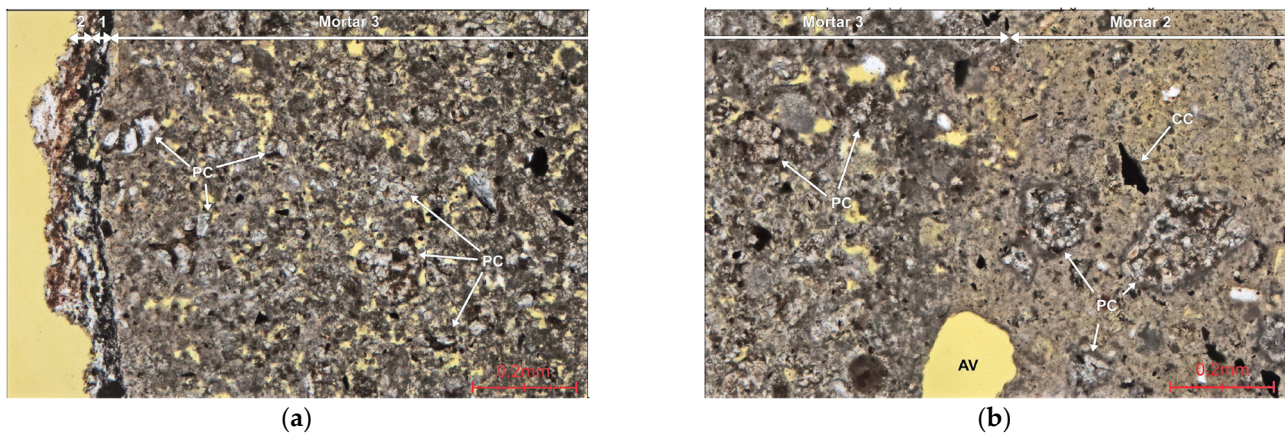


**Figure 9.** Micrographs in polarized light of CB5 sample: (a) the photo shows the paint layers on surface of the CB5-Ext (Mortar 3). The mortar is composed of Portland cement (PC) with a small amount of slaked lime added. The innermost paint layer (1) is of the same type as the carboniferous black paint layer in sample CB1. The outermost paint layer (2) consists of slaked lime and pigment of orange ochre; (b) the photo shows the contact between the CB5-Ext (Mortar3) and CB5-Int (Mortar 2). Compared to Mortar 3, Mortar 2 has a relatively high content of lime. Air voids = AV. Particles of charcoal = CC. The thin section was impregnated with yellow epoxy resin.

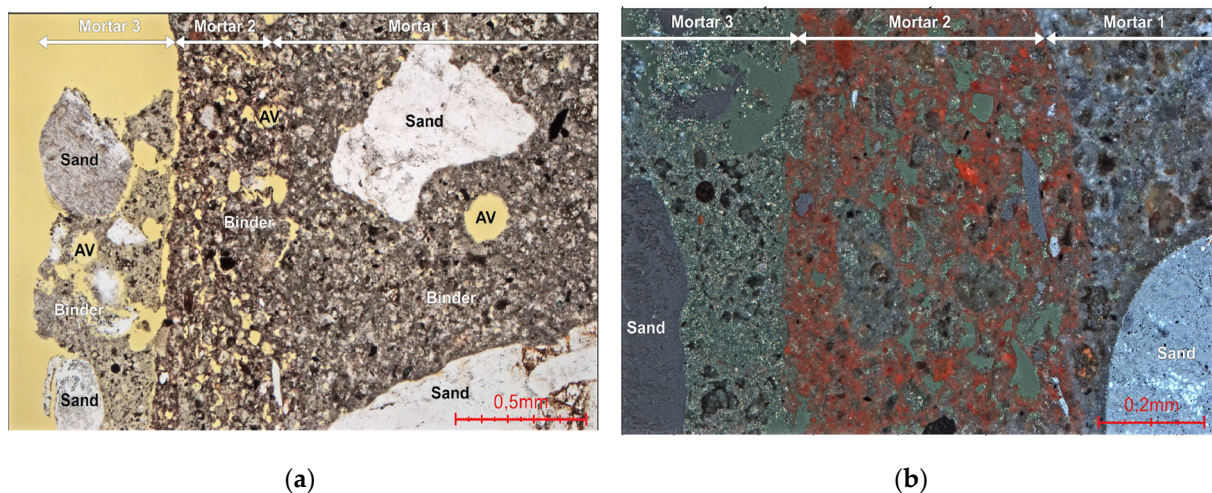


**Figure 10.** Micrographs in polarized light of CB11 sample: (a) the photo shows three mortar layers in the sample: Layer 1 (CB11-Int) is a Portland cement–lime mortar with blast furnace slags; Layer 2 is a reddish pigmented Portland cement–lime paste; Layer 3 (CB11-Ext) is remnants of relatively modern mortar with Portland cement.; (b) the photo shows the three mortar layers at a higher magnification and taken by use of reflected light microscopy. The pigment for Mortar 2 is red iron oxide. Air voids = AV. The thin section was impregnated with yellow epoxy resin.

A frequent presence in all samples of sub-angular partially hydrated clinker minerals of alite ( $C_3S$ ), belite ( $C_2S$ ), and ferrite ( $C_4AF$ ) proves that the Portland cement was the main binder of mortars used in the construction of Casa Barbot's. Some Portland cement clinker grains contain undifferentiated hydraulic calcium silicate phases and glass-like phases.

#### 4.4. Mechanical and Physical Properties

The results of mechanical and physical tests are presented in Tables 6 and 7, respectively. Due to the limitation in the number of samples, some were tested with no duplicates, while those with more than one tested sample are also presented as an average value together with the standard deviation (std).

**Table 6.** Compressive strength of Casa Barbot samples (std).

Sample Identification	Compressive Strength (MPa)	Mean Strength (MPa)
CB1	15.44	
CB2	55.70	
CB3	21.17	
CB4-1	17.98	14.25 (5.27)
CB4-2	10.52	
CB9-1	10.59	27.01 (14.4)
CB9-2	32.94	
CB9-3	37.50	
CB10-1	28.85	

**Table 7.** Density, open porosity, and capillary coefficient of CB samples (std).

Sample Identification	Real Density (kg/m <sup>3</sup> )	Open Porosity (%)	Capillarity Coefficient (kg/m <sup>2</sup> .min <sup>1/2</sup> )	
CB2	CB1-Ex	2482 (8.08)	21 (1.53)	0.47
	CB1-Int	2419 (40.07)	11.82 (0.05)	0.04
	CB2-2	2441 (9.96)	12.99 (0.85)	0.41
	CB2-3			0.20
	CB3-Int	2491	13.57	0.24
CB9	CB3-Ex	2501 (14.26)	16.84 (0.63)	0.30
	CB4	2350	11.47	0.28
	CB9-4	2478 (20.45)	21.43 (0.6)	1.51
	CB9-5			0.66
	CB10	2371	14.52	0.19

The real density of samples was in the range of 2350–2501 kg/m<sup>3</sup>. However, a large discrepancy can be observed in the samples taken from different parts of Casa Barbot, even in the duplicates, which hinders a decisive conclusion on the mechanical and physical properties of the mortars. This is because each sample is composed of several layers of mortars with different compositional, microstructural, and physical properties. CB2 possesses the highest strength among the others (55.7 MPa), due to the heterogeneous structure of CB2 that consists of different mortars and shapes (i.e., tree knot-like shape), see Table 1. CB2 also shows a relatively low capillary coefficient (0.3 kg/m<sup>2</sup>.min<sup>1/2</sup>) and low open porosity (13%) which corroborates the results of the mechanical test. This can be attributed to the high content of the binder in the composition of CB2, as was observed from XRD and XRF tests. On the other hand, high calcite content ensures the calcination of free lime during the lifetime of the sample and long-term strength gain. It seems that the largest content of gypsum is due to the addition of modern Portland cement during the intervention rather than its formation due to sulfation because the formed gypsum during the sulfation can lead to the loss of strength and adhesion [49]. CB1-Int shows the lowest capillary coefficient (0.04 kg/m<sup>2</sup>.min<sup>1/2</sup>) with a low open porosity of 11.82%. The incorporation of different materials such as Portland cement, blast furnace slag, limestone filler, and lime formed a compact structure (see Figure 8b) with lower capillary pores.

CB9 shows the highest open porosity among the mortars; however, it shows sensitivity to the test direction in both capillary water absorption and compressive tests. Although two samples of CB9 show high compressive strength (32.94 and 37.5 MPa), one of them registered the lowest value (10.59 MPa). Two distinct water absorption trends (Figure 11) and capillary coefficient (Table 7) were observed in CB9 replicates (1.51 and 0.66 kg/m<sup>2</sup>.min<sup>1/2</sup>). The longitudinal cracks in CB9-4 can be the main reason for the higher capillary coefficient

and lower compressive strength. This also accelerates the drying process in CB9-4, see Figure 11. CB1-Ex and CB9-4 show a very fast initial drying in comparison with the other samples. This can be well attributed to the high open porosity of these mortars (21% and 21.43%, respectively), accelerating the evaporation of absorbed water.

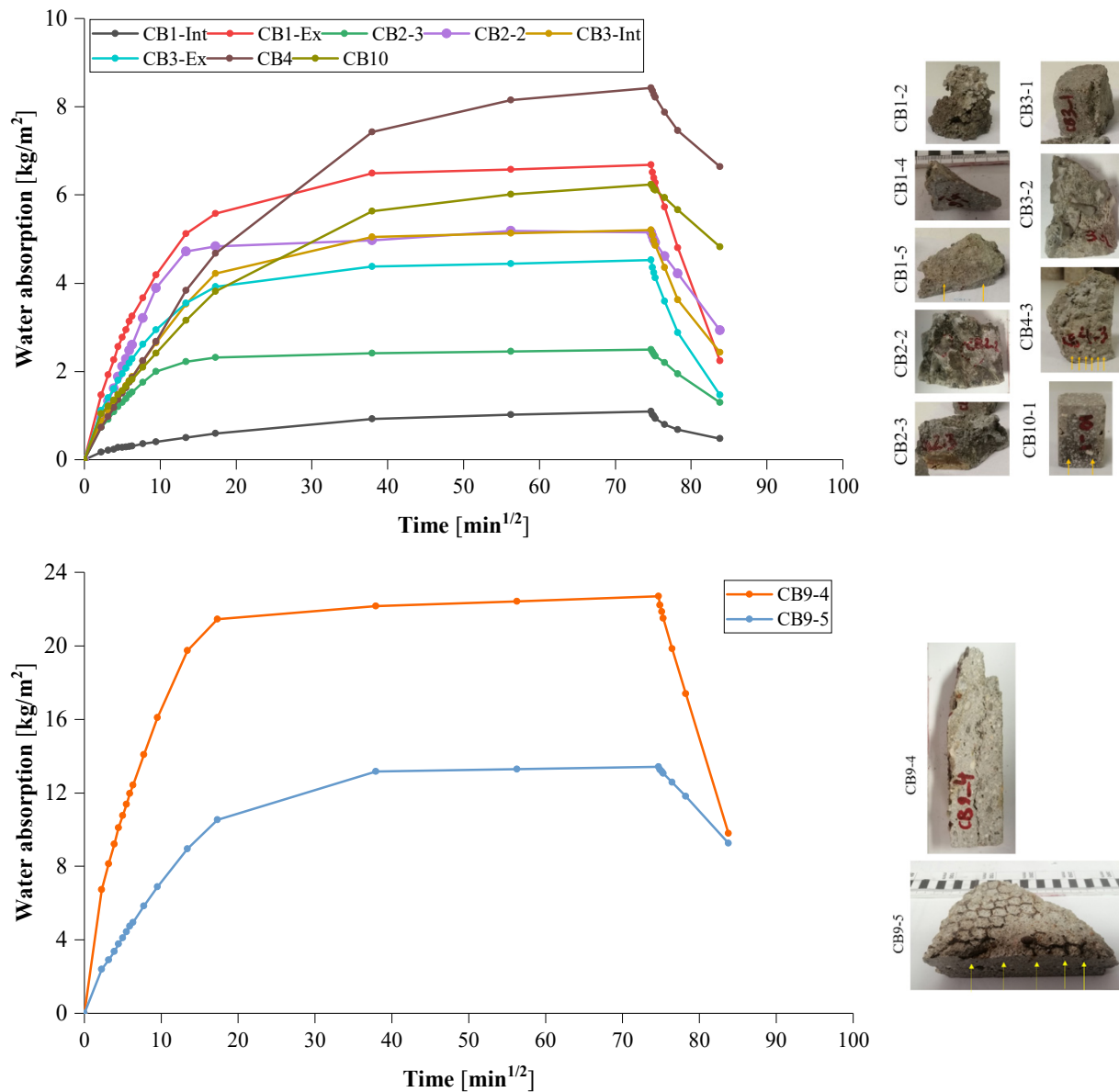


**Figure 11.** The water absorption and drying of mortars.

In a study conducted by Veiga et al. [3], the air lime used in the renders and plasters of Nossa Senhora da Luz, a fortress in Portugal, showed a compressive strength of as low as 1.7 N/mm<sup>2</sup>, with large capillary pore diameters causing a capillary coefficient of  $> \sqrt{5.46 \text{ kg/m}^2 \cdot \text{min}^{1/2}}$ . However, the compressive strength of mortars produced only with Portland cement (type I) was found to be about 62 MPa (at 28-day age) [50]. It was also observed that the addition of air lime can reduce the water resistance of mortar, while, the mix of cement and air lime leads to an increase in the strength of lime mortar from about 1 MPa (without cement) to 4.9 MPa with 10% cement [51]. In another study, the compressive strength of cement–lime (1:0.5:10, C:L:agg) was 19.6 MPa versus 1.8 MPa obtained for air lime mortar with the proportion of 1:3 stands for lime to aggregate ratio. In the same study, the capillary coefficient of cement–lime mortar was  $4.6 \text{ kg} \cdot \text{m}^{-2} \cdot \text{h}^{-1/2}$ .

## 5. Conclusions

The compositional characteristics of mortars used in the construction of decorative elements of the period garden of Casa Barbot, an Art Nouveau building in the Municipality of Vila Nova de Gaia, Portugal, were studied in this work using different techniques such as XRF, XRD, petrography, mechanical and physical tests. The results obtained allow the following conclusions:

- Different mortars were used in the construction of the cave structure. The mortars extracted from the different parts of the garden show diverse mineralogical and microstructural properties.
- Portland clinker minerals were identified by XRD in all mortars suggesting the use of Portland cement as the main binder employed, while other additives such as limestone filler, charcoal, blast furnace slags, and lime were also detected by petrography in some mortars. In addition to Portland cement, air lime and hydraulic lime seems to be present in the samples analyzed by petrography; the hydraulic lime was attributed to the presence of lumps and grains of lime with high content of impurities.
- Mortars of the external layers show higher levels of sulfation due to atmospheric urban exposure.
- Petrography analysis shows that the siliceous aggregates employed are similar in the analyzed mortars, which are mainly composed of quartz, quartzite, and feldspars.
- A large discrepancy was observed in the mechanical and physical properties of the mortars. In terms of open porosity, the mortars used in the external layers show higher porosity than those applied in the internal layers. Correspondingly, the capillary coefficient of external mortars shows the lowest capillary coefficient.
- There are no mortars with signs of abnormal transformation or deterioration.

These conclusions point to the inexistence of natural cement in the cast decorative elements of this construction, not confirming the suspicions of art historians that existed about its use.

**Author Contributions:** Conceptualization, H.M. and A.V.; methodology, H.M.; formal analysis, H.M.; investigation, H.M.; resources, A.V.; data curation, H.M. and A.S.S.; writing—original draft preparation, H.M.; writing—review and editing, A.S.S. and A.V.; supervision, A.V.; funding acquisition, A.V. All authors have read and agreed to the published version of the manuscript.

**Funding:** This research was funded by FCT, grant number POCI-01-0145-FEDER-031612.

**Institutional Review Board Statement:** Not applicable.

**Informed Consent Statement:** Not applicable.

**Data Availability Statement:** Not applicable.

**Acknowledgments:** The authors wish to thank Cristina Costa, the responsible architect of Casa Barbot and Câmara Municipal de Gaia for all the collaboration. The authors also would like to thank the Portuguese Foundation for Science and Technology (FCT) for the financial support within the scope of the Research Project CemRestore—Mortars for early 20th-century buildings conservation—Compatibility and Sustainability—POCI-01-0145-FEDER-031612.

**Conflicts of Interest:** The authors declare no conflict of interest.

## References

1. Gerardo, S.; Gonçalves, T.; Flores-Colen, I. Cimento Natural. História e Perspetivas de Uso Na Conservação de Edifícios Em Portugal. In Proceedings of the Conferência Património Industrial. Tradição, Inovação, Conservação, Lisboa, Portugal, 25 September 2015; LNEC: Lisboa, Portugal, 2015.
2. Varela, N.; Vieira, F.S. Cimento: Uma Matéria-Prima Essencial No Fabrico de Argamassas. In *Proceedings of the 1<sup>o</sup> Congresso Nacional de Argamassas de Construção, Lisbon, Portugal, 24–25 November 2005*; APFAC: Lisboa, Portugal, 2005; pp. 1–11.
3. Veiga, M.R.; Silva, A.S.; Tavares, M.; Santos, A.R.; Lampreia, N. Characterization of Renders and Plasters from a 16th Century Portuguese Military Structure: Chronology and Durability. *Restor. Build. Monum.* **2014**, *19*, 223–238. [[CrossRef](#)]

4. Silva, A.S.; Cruz, T.; Paiva, M.J.; Candeias, A.; Adriano, P.; Schiavon, N.; Mirão, J.A.P. Mineralogical and Chemical Characterization of Historical Mortars from Military Fortifications in Lisbon Harbour (Portugal). *Environ. Earth Sci.* **2011**, *63*, 1641–1650. [[CrossRef](#)]
5. Barbero-Barrera, M.D.M.; Maldonado-Ramos, L.; Van Balen, K.; García-Santos, A.; Neila-González, F.J. Lime Render Layers: An Overview of Their Properties. *J. Cult. Herit.* **2014**, *15*, 326–330. [[CrossRef](#)]
6. Veiga, R. Air Lime Mortars: What Else Do We Need to Know to Apply Them in Conservation and Rehabilitation Interventions? A Review. *Constr. Build. Mater.* **2017**, *157*, 132–140. [[CrossRef](#)]
7. Do Rosário Veiga, M.; Fragata, A.; Velosa, A.L.; Magalhães, A.C.; Margalha, G. Lime-Based Mortars: Viability for Use as Substitution Renders in Historical Buildings. *Int. J. Archit. Herit.* **2010**, *4*, 177–195. [[CrossRef](#)]
8. Elsen, J.; Balen, K.; Mertens, G. Hydraulicity in Historic Lime Mortars: A Review. In *Historic Mortars*; RILEM Bookseries; Springer: Dordrecht, The Netherlands, 2012.
9. Hurst, L. The Properties and Uses of Roman Cement. *Constr. Hist.* **2002**, *18*, 21–35.
10. Turismo e Lazer Fornos de Cal. Available online: <https://ufpm.pt/turismo-e-lazer/o-que-visitatar/80330/fornos-de-cal>. (accessed on 1 December 2022).
11. Mascarenhas-Mateus, J.; Castro, C. The Portland Cement Industry and Reinforced Concrete in Portugal. In Proceedings of the 6th International Congress on Construction History, Brussels, Belgium, 9–13 July 2018.
12. Weber, J.; Bayer, K.; Pintér, F. 19th Century “Novel” Building Materials: Examples of Various Historic Mortars under the Microscope. In *Proceedings of the 2nd Conference on Historic Mortars—HMC 2010 and RILEM TC 203-RHM Final Workshop, Prague, Czech Republic, 22–24 September 2010*; RILEM Publications SARL: Champs-sur-Marne, France, 2010; pp. 397–404.
13. Corrochano, C.M.; Ramírez-casas, J. Methodology of Identification of Natural and Historic Portland Cements. Application and Study in Mortars of Madrid and Barcelona. In Proceedings of the 5th Historic Mortars Conference, Pamplona, Spain, 12–21 June 2019.
14. Alvarez, J.; Sequeira, C.; Costa, M. Ensinamentos a Retirar Do Passado Histórico Das Argamassas. In *Proceedings of the 1º Congresso Nacional de Argamassas de Construção, Lisbon, Portugal, 24–25 November 2005*; APFAC: Lisboa, Portugal, 2005; p. 12.
15. Hughes, D.C.; Swann, S.; Gardner, A. Roman Cement: Part One: Its Origins and Properties. *J. Archit. Conserv.* **2007**, *13*, 21–36. [[CrossRef](#)]
16. Cantisani, E.; Falabella, A.; Fratini, F.; Pecchioni, E.; Vettori, S.; Antonelli, F.; Giamello, M.; Lezzerini, M. Production of the Roman Cement in Italy: Characterization of a Raw Material Used in Tuscany between 19th and 20th Century and Its Comparison with a Commercialized French Stone Material. *Int. J. Archit. Herit.* **2018**, *12*, 1038–1050. [[CrossRef](#)]
17. Hughes, D.C.; Jaglin, D.; Kozłowski, R.; Mayr, N.; Mucha, D.; Weber, J. Calcination of Marls to Produce Roman Cement. *J. ASTM Int.* **2007**, *4*, JAI100661. [[CrossRef](#)]
18. Vyskocilova, R.; Schwarz, W.; Mucha, D.; Hughes, D.; Kozłowski, R.; Weber, J. Hydration Processes in Pastes of Roman and American Natural Cements. *J. ASTM Int.* **2007**, *4*, JAI100669. [[CrossRef](#)]
19. Cazalla, O.; Rodriguez-Navarro, C.; Sebastian, E.; Cultrone, G.; De la Torre, M.J. Effects on Traditional Lime Mortar Carbonation. *J. Am. Ceram. Soc.* **2002**, *76*, 1070–1076.
20. Stefanidou, M.; Papayianni, I. The Role of Aggregates on the Structure and Properties of Lime Mortars. *Cem. Concr. Compos.* **2005**, *27*, 914–919. [[CrossRef](#)]
21. Faria, P.; Henriques, F.; Rato, V. Comparative Evaluation of Lime Mortars for Architectural Conservation. *J. Cult. Herit.* **2008**, *9*, 338–346. [[CrossRef](#)]
22. Weber, J.; Gadermayr, N.; Bayer, K.; Hughes, D.; Kozłowski, R.; Stillhammerova, M.; Ullrich, D.; Vyskocilova, R. Roman Cement Mortars in Europe’s Architectural Heritage of the 19th Century. In *Natural Cement*; ASTM International: West Conshohocken, PA, USA; Volume 1494 STP, 2008; pp. 69–83. ISBN 9780803134232.
23. Pintér, F.; Vidovszky, I.; Weber, J.; Bayer, K. Mineralogical and Microstructural Characteristics of Historic Roman Cement Renders from Budapest, Hungary. *J. Cult. Herit.* **2014**, *15*, 219–226. [[CrossRef](#)]
24. Gosselin, C.; Verges-Belmin, V.; Royer, A.; Martinet, G. Natural Cement and Monumental Restoration. *Mater. Struct. Constr.* **2009**, *42*, 749–763. [[CrossRef](#)]
25. Hughes, J.J.; Válek, J.; Groot, C.J.W.P. How to Identify a Natural Cement: Case Study of the Vassy Chureh, France. In *Historic Mortars Advances in Research and Practical Conservation*; Springer: Berlin/Heidelberg, Germany, 2019; ISBN 9783319916064.
26. Bratasz, L.; Kozłowski, R.; Mayr, N.; Mucha, D.; Stillhammerova, M.; Weber, J.; Chemistry, S.; Technology, R.; Vienna, A.A. Roman Cement-Key Historic Material to Cover the Exteriors of Buildings. In *RILEM Workshop Repair Mortars for Historic Masonry, Delft, The Netherlands, 26–28 January 2005*; RILEM Publications: Champs-sur-Marne, France, 2005; pp. 2–11.
27. Klisińska-Kopacz, A.; Tišlova, R.; Adamski, G.; Kozłowski, R. Pore Structure of Historic and Repair Roman Cement Mortars to Establish Their Compatibility. *J. Cult. Herit.* **2010**, *11*, 404–410. [[CrossRef](#)]
28. Velosa, A. Teatro Nacional de S. João (Porto, Portugal). Mortar Characterization in Early 20th Century Architecture. In Proceedings of the 3rd Historic Mortars Conference, Glasgow, UK, 11–14 September 2013.
29. Andrejkovičová, S.; Maljaee, H.; Rocha, D.; Rocha, F.; Soares, M.R.; Velosa, A. Mortars for Conservation of Late 19th and Early 20th Century Buildings—Combination of Natural Cements with Air Lime. *Materials* **2022**, *15*, 3704. [[CrossRef](#)]
30. Vaitkus, A.; Merkys, A.; Gražulis, S. Validation of the Crystallography Open Database Using the Crystallographic Information Framework. *J. Appl. Crystallogr.* **2021**, *54*, 661–672. [[CrossRef](#)]
31. Quirós, M.; Gražulis, S.; Girdzijauskaitė, S.; Merkys, A.; Vaitkus, A. Using SMILES Strings for the Description of Chemical Connectivity in the Crystallography Open Database. *J. Cheminform.* **2018**, *10*, 23. [[CrossRef](#)]

32. Merkys, A.; Vaitkus, A.; Butkus, J.; Okulič-Kazarinas, M.; Kairys, V.; Gražulis, S. COD::CIF::Parser: An Error-Correcting CIF Parser for the Perl Language. *J. Appl. Crystallogr.* **2016**, *49*, 292–301. [[CrossRef](#)]
33. Gražulis, S.; Merkys, A.; Vaitkus, A.; Okulič-Kazarinas, M. Computing Stoichiometric Molecular Composition from Crystal Structures. *J. Appl. Crystallogr.* **2015**, *48*, 85–91. [[CrossRef](#)] [[PubMed](#)]
34. Gražulis, S.; Daškevič, A.; Merkys, A.; Chateigner, D.; Lutterotti, L.; Quirós, M.; Serebryanaya, N.R.; Moeck, P.; Downs, R.T.; Le Bail, A. Crystallography Open Database (COD): An Open-Access Collection of Crystal Structures and Platform for World-Wide Collaboration. *Nucleic Acids Res.* **2012**, *40*, D420–D427. [[CrossRef](#)] [[PubMed](#)]
35. Gražulis, S.; Chateigner, D.; Downs, R.T.; Yokochi, A.F.T.; Quirós, M.; Lutterotti, L.; Manakova, E.; Butkus, J.; Moeck, P.; Le Bail, A. Crystallography Open Database—An Open-Access Collection of Crystal Structures. *J. Appl. Crystallogr.* **2009**, *42*, 726–729. [[CrossRef](#)] [[PubMed](#)]
36. Downs, R.T.; Hall-Wallace, M. The American Mineralogist Crystal Structure Database. *Am. Mineral.* **2003**, *88*, 247–250.
37. Veiga, M.R.; Magalhães, A.; Bosilikov, V. Capillarity Tests on Historic Mortar Samples Extracted from Site. Methodology and Compared Results. In Proceedings of the 13th International Brick and Block Masonry Conference, Amsterdam, The Netherlands, 4–7 July 2004.
38. Magalhães, A.; Veiga, M.R. Physical and Mechanical Characterisation of Ancient Mortars. Application to the Evaluation of the State of Conservation. *Mater. Construcción* **2008**, *59*, 61–77. [[CrossRef](#)]
39. Válek, J.; Veiga, M.R. Characterization of Mechanical Properties of Historic Mortars—Testing of Irregular Samples. *Adv. Archit. Ser.* **2005**, *20*, 365–374.
40. *BS EN 1015-11:2019*; Methods of Test for Mortar for Masonry. Determination of Flexural and Compressive Strength of Hardened Mortar. European Committee for Standardization: Brussels, Belgium, 2019; p. 18.
41. *EN 15801:2009*; Conservation of Cultural Property. Test Methods. Determination of Water Absorption by Capillarity. European Committee for Standardization: Brussels, Belgium, 2009.
42. *EN 1936:2006*; Natural Stone Test Methods; Determination of Real Density and Apparent Density, and of Total and Open Porosity. European Committee for Standardization (CEN): Brussels, Belgium, 2006.
43. Do Rosário Veiga, M.; Santos Silva, A. Mortars. In *Long-term Performance and Durability of Masonry Structures*; Elsevier: Amsterdam, The Netherlands, 2019; pp. 169–208.
44. Van Hees, R.P.J.; Binda, L.; Papayianni, I.; Toubakari, E. Characterisation and Damage Analysis of Old Mortars. *Mater. Struct.* **2004**, *37*, 644–648. [[CrossRef](#)]
45. Crammond, N.J. Thausamine in Failed Cement Mortars and Renders from Exposed Brickwork. *Cem. Concr. Res.* **1985**, *15*, 1039–1050. [[CrossRef](#)]
46. Ludwig, U.; Mehr, S. Destruction of Historical Buildings by the Formation of Ettringite and Thaumasite. In Proceedings of the 8th International Congress on the Chemistry of Cement, Rio de Janeiro, Brazil, 22–27 September 1986; Volume 5, pp. 181–188.
47. Collepari, M. Thaumasite Formation and Deterioration in Historic Buildings. *Cem. Concr. Compos.* **1999**, *21*, 147–154. [[CrossRef](#)]
48. Engström, F.; Adolfsson, D.; Samuelsson, C.; Sandström, Å.; Björkman, B. A Study of the Solubility of Pure Slag Minerals. *Miner. Eng.* **2013**, *41*, 46–52. [[CrossRef](#)]
49. Tian, B.; Cohen, M.D. Does Gypsum Formation during Sulfate Attack on Concrete Lead to Expansion? *Cem. Concr. Res.* **2000**, *30*, 117–123. [[CrossRef](#)]
50. Malaiskiene, J.; Skripkiunas, G.; Vaiciene, M.; Karpova, E. The Influence of Aggregates Type on W/C Ratio on the Strength and Other Properties of Concrete. *IOP Conf. Ser. Mater. Sci. Eng.* **2017**, *251*, 012025. [[CrossRef](#)]
51. Gulbe, L.; Vitina, I.; Setina, J. The Influence of Cement on Properties of Lime Mortars. *Procedia Eng.* **2017**, *172*, 325–332. [[CrossRef](#)]

**Disclaimer/Publisher’s Note:** The statements, opinions and data contained in all publications are solely those of the individual author(s) and contributor(s) and not of MDPI and/or the editor(s). MDPI and/or the editor(s) disclaim responsibility for any injury to people or property resulting from any ideas, methods, instructions or products referred to in the content.